The Journal of Engine Research

Journal Homepage: www.engineresearch.ir

Evaluation of the Effects of Equivalence Ratio on the Combustion in an HCCI Engine

M. Rabeti[1], O. Jahanian[2*], A. Ranjbar[3], S. M. Safieddin Ardebili[4], H. Solmaz[5]

[1] *Babol Noshirvani University of Technology, Babol, Iran, masoud.rabeti@gmail.com*
[2] *Babol Noshirvani University of Technology, Babol, Iran, jahanian@nit.ac.ir*
[3] *Babol Noshirvani University of Technology, Babol, Iran, ranjbar@nit.ac.ir*
[4] *Shahid Chamran University of Ahvaz, Ahvaz, Iran, m.safieddin@scu.ac.ir*
[5] *Gazi University, Ankara, Turkey, hsolmaz@gazi.edu.tr*
[*] *Corresponding Author*

ARTICLE INFO

Article history:
Received: 5 December 2020
Accepted: 16 January 2021

Keywords:
HCCI Combustion
3D-CFD Simulation
Equivalence Ratio
LTRHR
HTRHR

ABSTRACT

In this paper, the influence of the equivalence ratio on combustion characteristics has been examined by considering 16 different operating conditions. The fuel used in this research is gasoline and the ignition takes place in two stages. The first stage of combustion is due to low-temperature reaction heat release (LTRHR), and the second stage is related to the high-temperature reaction heat release (HTRHR). The three-dimensional computational fluid dynamics (3D-CFD) with chemical kinetics has been chosen as the numerical method. In all of the studied operating conditions, the 3D-CFD simulations were able to see the combustion properly and the increase of maximum pressure and maximum rate of heat release ($ROHR_{max}$) with the rise of the equivalence ratio was properly observed. Also, by increasing the equivalence ratio, the 3D-CFD model show advanced maximum pressure and $ROHR_{max}$ but mistakenly predicted the start of LTRHR more delayed, while the HTRHR was properly predicted.

1) Introduction

Nowadays, most of the required power for transportations is supplied by conventional internal combustion engines (ICEs), including spark ignition (SI) and compression ignition (CI) engines.

The fuel consumption rate, efficiency, and emission levels are important factors in ICEs. Low-temperature combustion (LTC) engines are one of the promising technologies designed by considering the importance of efficiency, environmental pollution, and fuel consumption.

Homogeneous charge compression ignition (HCCI) engines are one variant of the LTC engines that are designed by combining the combustion processes of conventional ICEs. In the HCCI engines, the poor premixed air-fuel mixture enters the combustion chamber, and during the compression stage, due to the rise of temperature in this mixture, auto-ignition occurs in the combustion chamber.

This combustion process in the HCCI engines presents better engine performance than the engines with other combustion strategies. High thermal efficiency and low levels of soot emission are some of the advantages and having a limited operating range and being unable to control the start of combustion are some of the limitations of the HCCI engines.

One of the other significant advantages of the HCCI engines is that these engines do not require another production line, and this technology can be achieved by adding some auxiliary equipment and some modifications in the production line of conventional ICEs [1-5].

Investigating the effects of important parameters in an engine, controlling the combustion process, analyzing the behavior of influential parameters on combustion, and optimizing the engine performance in different operating conditions are some of the goals that can be obtained by experimental and numerical studies [6, 7].

The usage of different fuels and the behavior of important parameters on combustion, fuel consumption, and the emissions of HCCI engines are some of the topics that the researchers have experimentally examined.

Lu et al. [8] examined the auto-ignition and combustion characteristics in an HCCI engine that worked by a mixture of ethanol and n-heptane fuels. The results showed that by using ethanol and n-heptane, the maximum mean effective pressure increases from 3.38 bars to 5.1 bars, and while in high engine speeds, the indicated thermal efficiency can be raised to 50%, in low engine speeds, the thermal efficiency decreases.

Maurya and Agarwal [9] studied the impacts of air inlet temperature and air-fuel ratio on the cycle-to-cycle variations of combustion in the HCCI engines. They stated that the maximum rate of pressure rises and the coefficient of variations (COV) of indicated mean effective pressure are critical parameters that can define the operating range of an HCCI engine.

The influences of iso-propanol and n-heptane fuel mixture on combustion specifications of HCCI engines and the performance of these engines were analyzed in the work of Ipci et al. [10]. These researchers concluded that increasing iso-propanol delays the start of combustion (SOC) while reducing the combustion duration.

Cinar et al. [11] evaluated the influence of the air inlet temperature on the engine performance and combustion in a gasoline-fueled HCCI engine. The results suggested that increasing the air inlet temperature leads to higher in-cylinder pressures and ROHR, but decreasing the combustion duration.

Polat [12] carried out a study on HCCI engines. The used fuel in this research was a mixture of diethyl ether and ethanol. In this study, the in-cylinder pressure, ROHR, indicated mean effective pressure (IMEP), and the combustion duration was analyzed. It was observed that higher λ values could result in lower in-cylinder pressures and ROHR. It was also shown that the combustion duration rises by increasing the air inlet temperature.

Calam et al. [13] evaluated the influences of the compression ratio on combustion in HCCI engines. The results showed that by increasing the compression ratio, the combustion duration decreases. Moreover, longer combustion durations were observed by increasing the fuel octane number.

Because of the complications of the combusted fluid flow in the combustion chamber, for analyzing the effective parameters on the performance of the engine, accurate examinations require a 3D-CFD simulation that considers the chemical kinetics. Different problems can be analyzed by CFD codes.

These codes can use various approaches to generate an accurate grid. For solving the problems, different initial and boundary

conditions and also multiple sub-models are used by the CFD codes. Considering the rise of computational power, the computer codes and software programs such as AVL FIRE, KIVA, Open FOAM, and CONVERGE CFD are employed for simulating the fluid flow, the combustion process, and the emissions in the engines [14-16].

Numerous research studies have used 3D-CFD simulations for evaluating the influence of important parameters in HCCI engines, and here are some of these studies:

Ognik and Colovitchev [17] numerically analyzed the effects of changing the engine speed, air-fuel ratio, and valve timing on the performance of HCCI engines using 3D-CFD simulations that considered detailed chemical kinetics. These researchers used AVL FIRE software for the 3D-CFD simulation, and they employed chemical kinetics that included 479 chemical reactions and 101 chemical species. The comparison of their simulation results with the experimental data showed an error of 1-10%.

Noel et al. [18] used a 3D-CFD approach that considered chemical kinetics to examine an HCCI engine with n-heptane fuel. In this research, for analyzing the combustion in the engine, reduced chemical kinetics was used along with Star-CD/Kinetics combustion CFD code.

The reduced chemical kinetics included 37 chemical species and 61 chemical reactions. The simulation results for different rates of exhaust gas recirculation (EGR) showed that for a constant gas temperature, dilution of the air-fuel mixture with the EGR retards the ignition timing.

In a study carried out by Wang et al. [19], the combustion in an HCCI engine was numerically analyzed. This numerical study was performed by the 3D-CFD method in AVL Fire software and the Chemkin chemical kinetics program. The fuel used in this research was gasoline. These software packages were employed to simulate the injection and combustion and the production process of the emissions.

Poorghasemi [20] performed a 3D-CFD analysis coupled with reduced chemical kinetics on an HCCI engine. The used fuel in their research was natural gas (NG). The reduced mechanism included 26 species and 63 reactions. The in-cylinder pressure, maximum pressure, gross IMEP, and accumulated heat release rate were selected as the parameters for analyzing the reduced mechanism. They showed that the studied reduced mechanism is valid for the combustion and appropriate for estimating the operating characteristics.

In a research study performed by Yousefzadeh and Jahanian [21], the combustion process of an HCCI engine was analyzed by 3D-CFD simulations coupled with detailed chemical kinetics. The used fuel in this research was NG. This research aimed to examine the effective parameters for adjusting the combustion process in an HCCI engine. The results indicated that by changing the concentration of hydroxyl radicals (OH), the combustion phase can be altered.

So far, different studies have been carried out on evaluating the influences of different parameters in HCCI engines. To the best of the authors' knowledge, there is no study that numerically and experimentally investigated the effect of equivalence ratio on the time of occurrence of combustion parameters such as LTRHR, HTRHR, the maximum pressure (P_{max}), $ROHR_{max}$, and rate of iso-octane and n-heptane in a wide operating condition in HCCI engines.

2) The Experimental Setup and Procedures

Table 1 and Figure 1 show the characteristics and schematics of the examined engine in this research, respectively. This test engine is a four-stroke single-cylinder Ricardo Hydra engine.

Table 1: Specifications of the HCCI engine

Bore	80.26 (mm)
Stroke	88.90 (mm)
Compression ratio	5:1 – 13:1
IVC	56 °CA ABDC
EVO	56 °CA BBDC

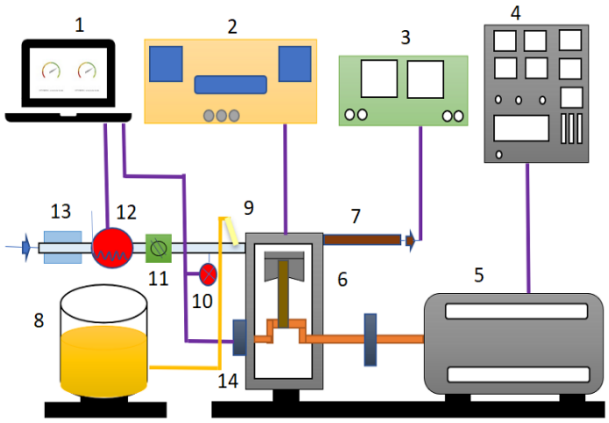

Figure 1: Test setup
1- Computer, 2- Combustion analysis device, 3- Gas analyzer, 4- Dynamometer control, 5- DC Dynamometer, 6- HCCI engine, 7- Exhaust, 8- Fuel tank, 9- Injector, 10- Thermocouple, 11- Throttle valve, 12- Air heater, 13- Airflow measurement device, 14- Encoder

During the tests with the test engine, the amount of fuel was adjusted with a fuel control system and it was injected into the inlet manifold through an injection system. A system equipped with a potentiometer was used to keep the equivalence ratio constant. The used fuel tank in this setup had a precision of 0.01 g. Also, a McClure brand electrical type dynamometer was employed on this setup.

A K-type thermocouple was used to measure the air inlet temperature. For evaluating the in-cylinder pressure, a Kistler 6121 piezoelectric with a precision of 0.5% and the operating range of 0-250 bars was employed. The pressure values were recorded every 0.36° CA. Furthermore, to collect raw in-cylinder pressure signals a Cussons P4110 combustion analysis device was used.

The analog pressure signals were changed to digital signals using the National instrument USB 6259 device. A line drive encoder with 1000 pulses in each CA rotation was connected to the crank angle and it produced a signal for locating the piston location every 0.36° CA. In each experimental state, the pressure values were averaged for 50 successive cycles.

The examined engine was initially in the SI state, but it was set in the HCCI state by setting the cooling water temperature and oil temperature constant at 343 K and 333 K, respectively. In this study, gasoline fuel with an Octane number of 20, which is a mixture of 20% iso-octane (C_8H_{18}) and 80% n-heptane (C_7H_{16}), was used.

The experiments in this research were conducted in 16 different operating conditions with a constant air inlet temperature of 313 K, a constant compression ratio of 12, and various engine speeds and equivalence ratios. The operating conditions for these tests are tabulated in Table 2.

Table 2: The operating conditions for the tests

Speed (rpm)	Equivalence ratio	Speed (rpm)	Equivalence ratio
800	0.31	1200	0.34
	0.39		0.40
	0.50		0.53
	0.62		0.58
1000	0.32	1400	0.35
	0.41		0.41
	0.54		0.46
	0.61		0.55

Finally, the ROHR was calculated using the developed MATLAB code based on the first law of thermodynamics [22].

3) The Numerical Approaches and Procedures

The 3D-CFD simulations were conducted using the AVL Fire commercial software coupled with chemical kinetics. In the 3D model, the continuity, Navier-Stokes, energy, and the equations for the mass fraction of species were solved.

Also, for modeling, the turbulence of the flow, the k-ε turbulence equations were used. The species mass fractions were obtained from the chemical kinetics. The solving algorithm of these equations has been shown in Figure 2. The equations as mentioned earlier are respectively presented, as follows [21, 23]:

$$\frac{\partial \rho}{\partial t} + (\nabla . \rho U) = 0 \tag{1}$$

$$\frac{D(\rho U_i)}{Dt} = \rho g_i - \frac{\partial P}{\partial x_i} + \frac{\partial}{\partial x_j}\left[\mu\left(\frac{\partial U_i}{\partial x_j} + \frac{\partial U_j}{\partial x_i} - \frac{2}{3}\frac{\partial U_k}{\partial x_k}\delta_{ij}\right) - \rho\overline{u_i' u_j'}\right] \tag{2}$$

$$\frac{D(\rho H)}{Dt} = \rho \dot{q}_g + \frac{\partial P}{\partial t} + \frac{\partial}{\partial x_i}\left(U_j \tau_{ij}\right) + \frac{\partial}{\partial x_j}\left(\lambda \frac{\partial T}{\partial x_j}\right) \tag{3}$$

$$\frac{D(\rho C)}{Dt} = \rho \dot{r} + \frac{\partial}{\partial x_j}\left(D\frac{\partial C}{\partial x_j} - \rho\overline{cu_i}\right) \tag{4}$$

$$\frac{D(\rho k)}{Dt} = P + G - \varepsilon + \frac{\partial}{\partial x_j}\left(\mu + \frac{\mu_t}{\sigma_k}\frac{\partial k}{\partial x_j}\right) \tag{5}$$

$$\frac{D(\rho \varepsilon)}{Dt} = \left(C_{\varepsilon 1}P + C_{\varepsilon 2}G + C_{\varepsilon 4}k\frac{\partial U_k}{\partial x_k} - C_{\varepsilon 2}\varepsilon\right)\frac{\varepsilon}{k} + \frac{\partial}{\partial x_j}\left(\frac{\mu_t}{\sigma_\varepsilon}\frac{\partial \varepsilon}{\partial x_j}\right) \tag{6}$$

$$P = -2\mu_t S : S - \frac{2}{3}[\mu_t (trS) + k](trS) \tag{7}$$

$$S = \sqrt{2\Omega_{ij}\Omega_{ij}} \tag{8}$$

$$\Omega_{ij} = \frac{1}{2}\left(\frac{\partial U_i}{\partial x_j} - \frac{\partial U_j}{\partial x_i}\right) \tag{9}$$

$$G = -\frac{\mu_t}{\rho \sigma_p}\nabla \rho \tag{10}$$

$$\mu_t = C_\mu \rho \frac{k^2}{\varepsilon} \tag{11}$$

The constant values in Eq. (6) have been presented in Table 3.

Table 3: The constant values in the turbulence equation [23]

C_μ	$C_{\varepsilon 1}$	$C_{\varepsilon 2}$	$C_{\varepsilon 3}$	$C_{\varepsilon 4}$	σ_k	σ_ε	σ_p
0.09	1.44	1.92	0.8	0.33	1	1.3	0.9

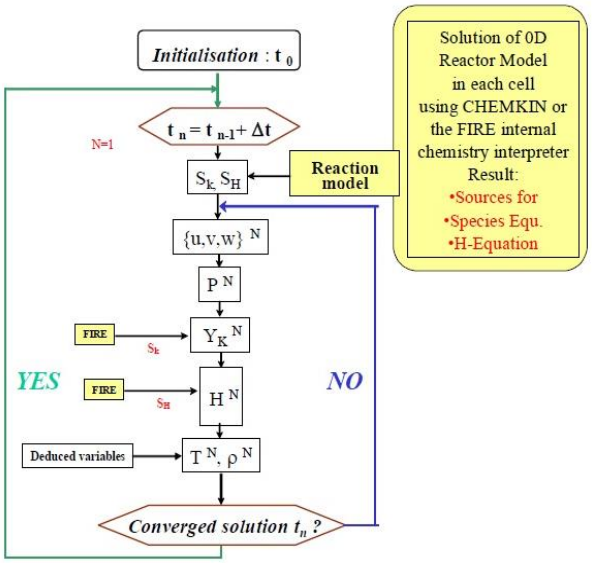

Figure 2: The coupling algorithm of the chemical kinetics and the governing equations on the 3D model in the FIRE software [23]

In this research, the reduced mechanism of gasoline, which included 296 reactions and 73 chemical species, was used for simulating chemical kinetics [24].

As it was mentioned, the mass fractions of species were obtained from the chemical kinetics. The combustion chamber of an ICE can be considered as a control volume from IVC until the EVO. In a closed system, chemical reactions are the only reason for changing the concentration of each chemical species. A reaction with a third body, the reaction rate, the reaction constant, and the chemical species production rate can be presented respectively, as follow [25]:

$$\sum_{k=1}^{N_s} \nu'_{k,i} M_i + TB \leftrightarrow \sum_{k=1}^{N_s} \nu''_{k,i} M_i + TB \tag{12}$$

$$RR_i = \left[\sum_{k=1}^{N_s} (a_{k,i})(TB_k)\right] \left[k_{f,i} \prod_{k=1}^{N_s} (M_k)^{\nu'_{k,i}} - k_{b,i} \prod_{k=1}^{N_s} (M_k)^{\nu''_{k,i}}\right] \tag{13}$$

$$k = AT^{\beta} e^{-\left(\frac{E_a}{R_u T}\right)} \tag{14}$$

$$\dot{\omega}_k = \sum_{i=1}^{N_R} RR_i \left(\nu'_{k,i} - \nu''_{k,i}\right) \tag{15}$$

Before validating the model, mesh and time-step independence tests were carried out for the 3D-CFD simulations. To examine mesh independence, meshing was done by four different cell sizes.

The number of mesh has been presented in Table 4. Due to the homogeneity of the mixture and geometrical symmetry of the piston bowl, a 45° sector of the combustion chamber was selected for further analysis. Figure 3 illustrates the generated mesh structure.

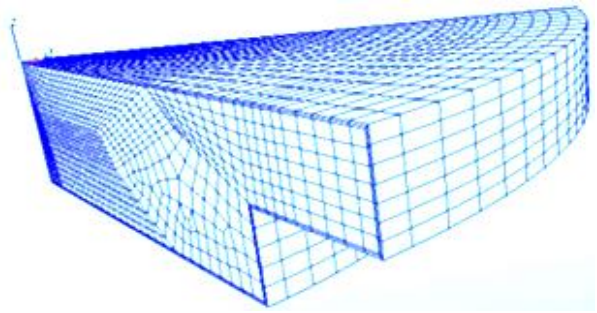

Figure 3: The selected mesh at TDC

Table 4: Number of cells at TDC

Mesh 1	7764
Mesh 2	13656
Mesh 3	26516
Mesh 4	32488

To compare the generated meshes, the test engine was analyzed by the CFD method in a constant state. The in-cylinder pressures for four different generated meshes were evaluated and Mesh 3 was selected for the simulations.

To examine the time-step independence and select the best time-step size, several time-step sizes were tested while keeping the operating condition constant. For this purpose, five different time-step sizes of 1, 0.5, 0.2, 0.1, and 0.09° CA were tested. The in-cylinder pressure results based on different crank angles and with different time-step sizes have been evaluated and the time-step size of 0.1° CA was selected.

After performing the mesh and time-step size independence tests, the 3D-CFD model was validated. To validate the simulation results, the results from the 3D-CFD model coupled with chemical kinetics were compared with the experimental results. This comparison has been presented in Figure 4.

These results were obtained with the air inlet

temperature of 313 K, the compression ratio of 12, the engine speed of 800 rpm, using gasoline fuel with an octane number of 20, an equivalence ratio of 0.62 for (a), and an equivalence ratio of 0.39 for (b). As can be observed, the results of the 3D-CFD model are in good compatibility with the experimental results.

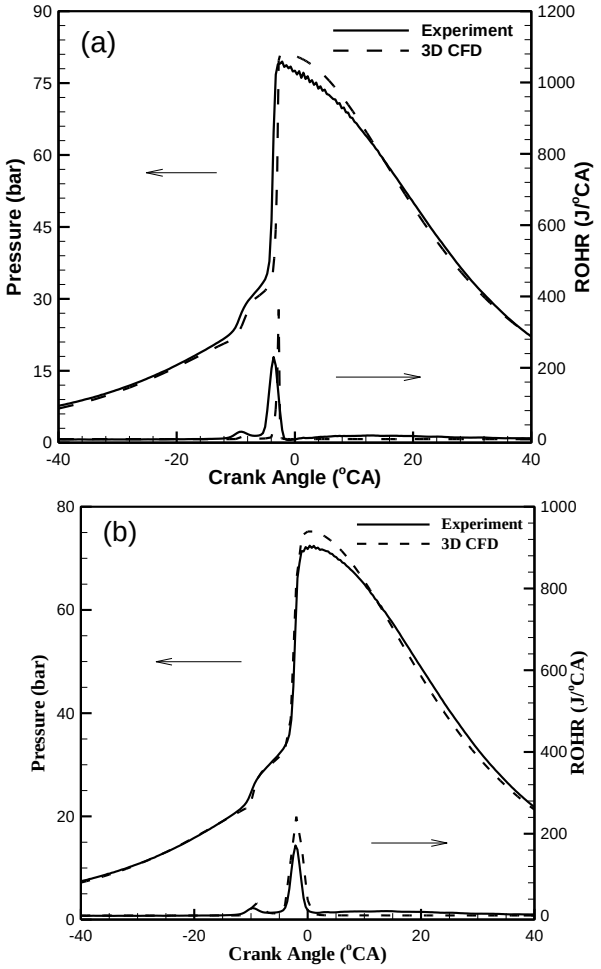

Figure 4: Comparison of the in-cylinder pressure and ROHR from the 3D-CFD model and the experimental tests.

4) Results and Discussion

As explained before, the combustion in HCCI engines depends on the history of in-cylinder pressure and temperature. Also, the changes in the in-cylinder pressure and ROHR due to crank angle are connected to the air-fuel mixture and the in-cylinder temperature.

The used fuel in this research is a mixture of iso-octane and n-heptane. These two fuels have different combustion behaviors in terms of ROHR and SOC.

Thus, the ignition of the used fuel mixture happens in two stages. Therefore, the changes in the in-cylinder pressure and the ROHR are different from those with the fuels that have one stage of ignition. Two-stage ignition can be noticed from the behavior of the in-cylinder pressure and ROHR. In every stage an ascending state is created in the plot, so with the fuels with one stage of ignition, there are just one of these increases. On the other hand, with the fuel mixtures with two stages of ignition, this increase happens two times. These two stages are attributed to the LTR heat release and HTR heat release, respectively.

Figure 5 depicts the changes of in-cylinder pressure and ROHR for all 16 operating states of the engine that were experimentally tested. As was mentioned before, these tests were conducted in a broad range of engine speed (N=800, 1000, 1200, and 1400 rpm) and with different air-fuel ratios, which are defined as equivalence ratios.

These experimental results indicate that with higher equivalence ratios, the maximum in-cylinder pressure and the maximum ROHR increase. Also, with higher values of equivalence ratio, both stages of ignition happen earlier.

The reason for this behavior is that with higher equivalence ratios, the fuel mass and the heat released from the combustion increase.

This behavior can be observed for all 16 examined states in this research. It is noteworthy that in the compression stage since the ignition and heat release are not started yet, the in-cylinder pressure trend for all of the equivalence ratios are identical. From the ROHR plot, it can be noticed that in this range, the same similarity exists for the ROHR results with different equivalence ratios.

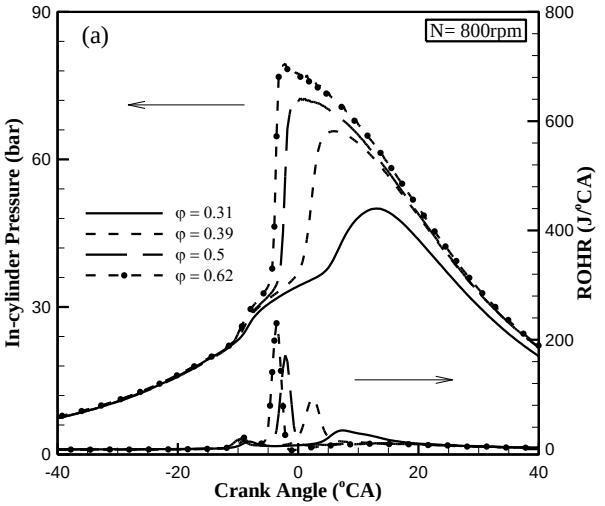

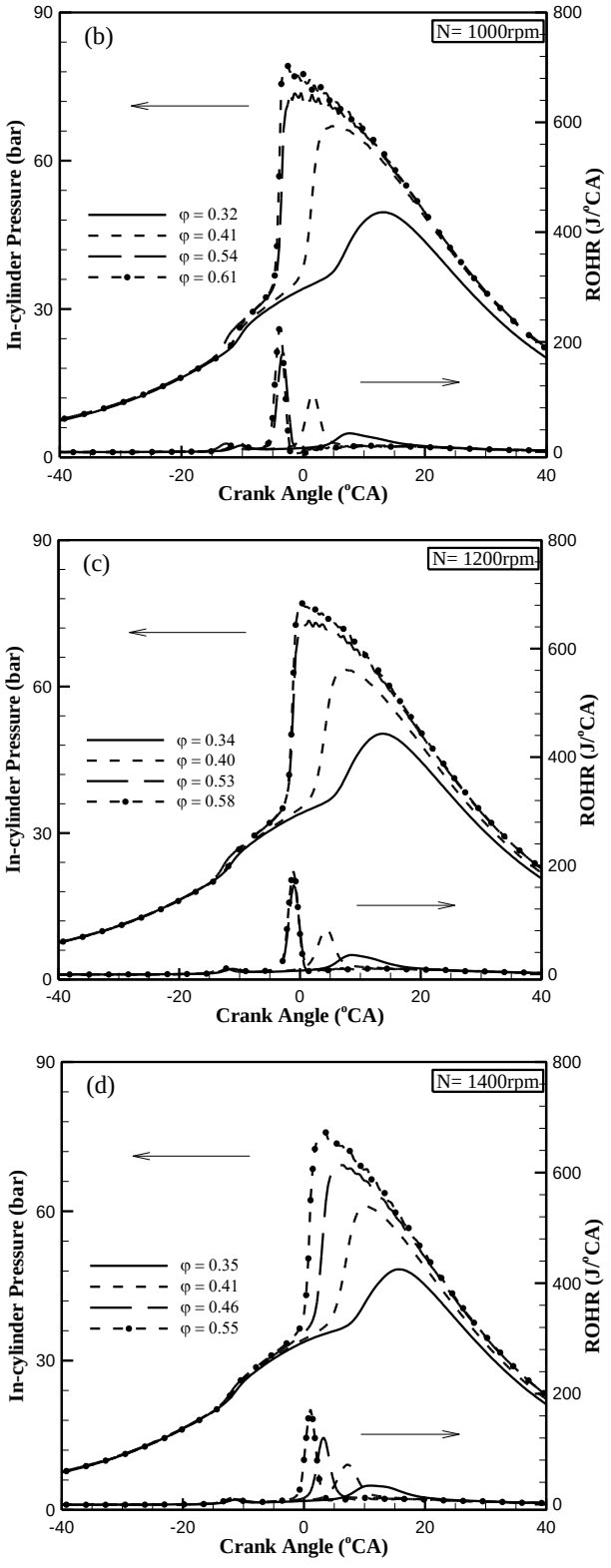

Figure 5: The experimental results for the ROHR and in-cylinder pressure based on the crank angle

Figure 6 shows the results from the 3D-CFD model for the changes in the in-cylinder pressure and ROHR based on the crank angle in different equivalence ratios and engine speeds.

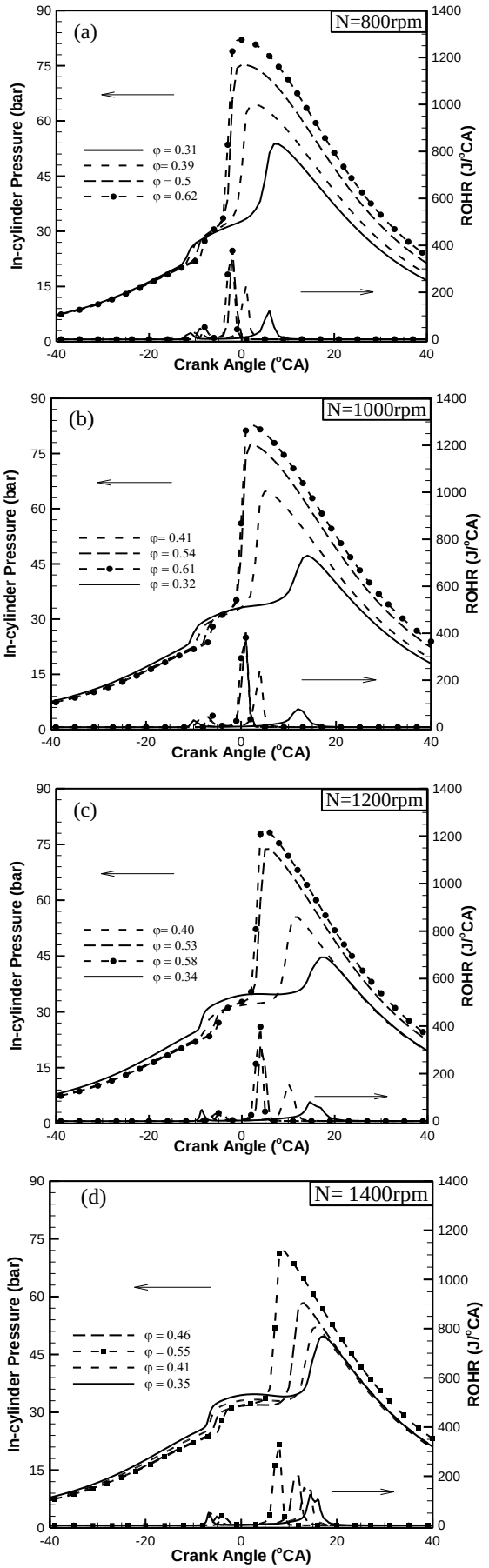

Figure 6: 3D-CFD model results for the In-cylinder pressure and ROHR based on different crank angles

As it can be noticed from the plots, this model predicted the two-staged combustion in all of the cases. Also, it was observed that by increasing the equivalence ratio, the pressure and ROHR increase. Even though with higher equivalence ratios, the model exhibited an insignificant error in determining the start of LTRHR; the start of HTRHR and the overall trend of the combustion were correctly predicted.

As it is said that in this study, gasoline which is the mix of iso-octane and n-heptane was used, and also the octane number of gasoline was 20 and which means that the fuel was formed of 20% iso-octane and 80% n-heptane.

The time of ignition for both iso-octane and n-heptane is different and as a result of the fact, the gasoline has ignited in two distinct steps.

Since the octane number of n-heptane is zero and it bears no resistance against ignition, it burns earlier and initiates the first step of ignition. Iso-octane is a type of fuel with the octane number 100 which shows high resistance against ignition; Therefore, it burns later and it causes the second stage of ignition to form.

Figure 7 illustrates the effect of ignition of iso-octane and n-heptane on the first and second stages of ignition. The impact of the ignition of iso-octane and n-heptane on the trend of pressure is recognizable. Whenever the rate of n-heptane reaches its maximum, the first increasing trend of pressure creates, and as the rate of iso-octane hits its peak, the second upward trend of pressure creates.

It is necessary to declare that the rate of n-heptane is more than the iso-octane rate and the reason behind this behavior is that when the octane number of gasoline is 20, the amount of n-heptane is higher in comparison with the iso-octane.

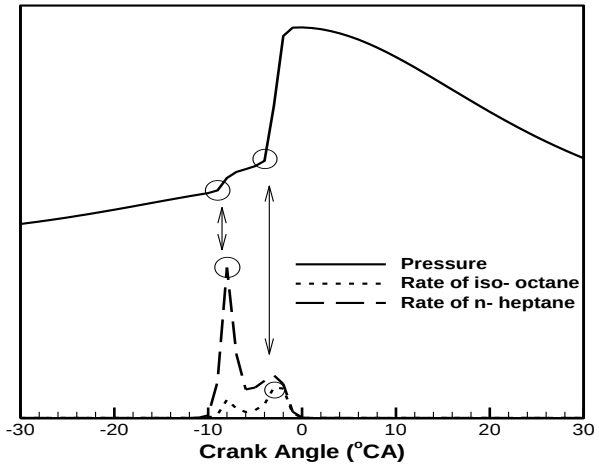

Figure 7: Influence of the maximum rate of iso-octane and n-heptane on two stages heat release in pressure trend

Figure 8 depicts the effect of equivalence ratio on the variation of the rate of iso-octane and n-heptane consumption versus crank angle for 16 operating conditions.

The result of Figure 8 has been earned via 3D-CFD simulation and could not see these results in experimental tests. As it can be seen, in all different circumstances, the maximum rate of n-heptane consumption happens sooner compared to the highest peak of iso-octane.

From a technical viewpoint, with increasing equivalence ratio, the amount of fuel rises and it is expected that the start of both stages of ignition occurs beforehand.

Figure 8 clears that with rising equivalence ratio the maximum rate of iso-octane consumption occurs earlier although the highest peak of n-heptane shapes later which is against the experimental results. Because in the 3D-CFD model, the start of the first stage of ignition (LTRHR) is recognized by the maximum n-heptane consumption rate, a detailed mechanism thoroughly covering the initial reaction is needed. The mistake could be related to the examined reduced mechanism.

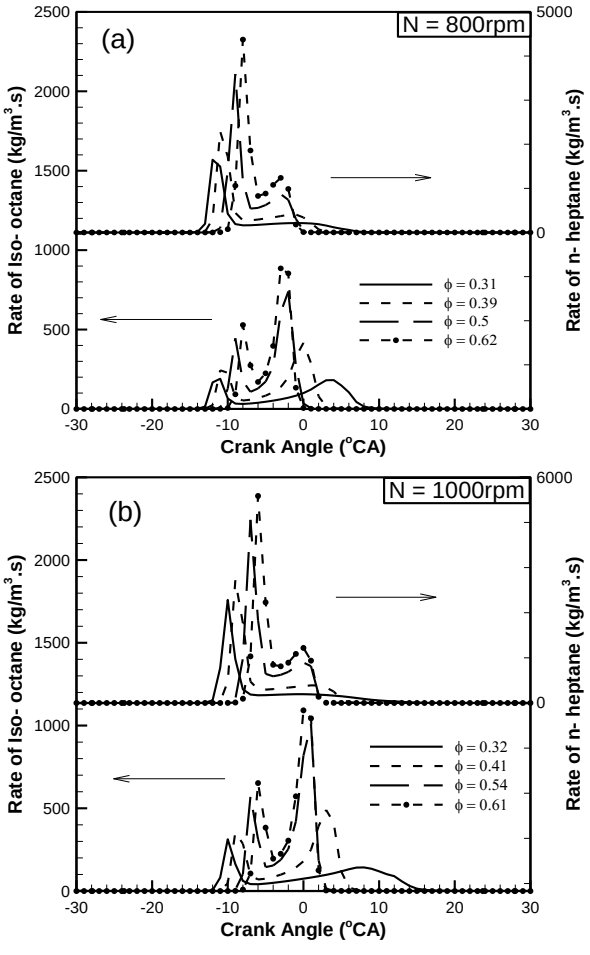

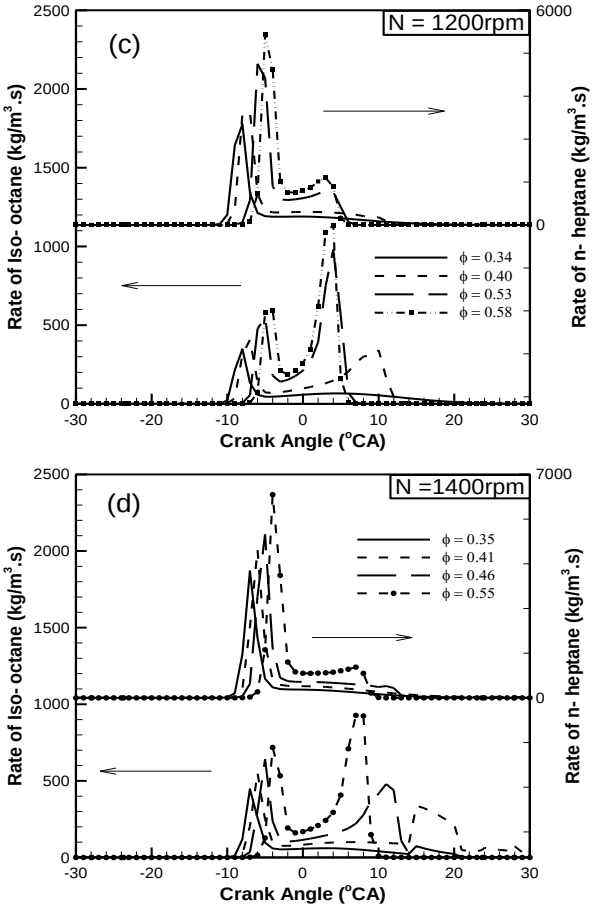

Figure 8: Variation of the rate of iso-octane and n-heptane via crank angle

Concerning the two stages of ignition which were mentioned above and also the results obtained till now, a reasonable definition for recognizing LTRHR and HTRHR will be offered quantitatively. LTRHR and HTRHR are considered as the first and second steps of ignition respectively. In this study, when the amount of ROHR ($dQ/d\theta$) reaches 3 , it is introduced as the start of LTRHR and whenever the derivation of ROHR ($d^2Q/d\theta^2$) goes beyond 40 J/deg^2, it is introduced as the start of HTRHR. The definitions of LTRHR and HTRHR are depicted schematically in Figure 9.

In Figure 10., LTRHR and HTRHR are checked for all the operating conditions for both experiments and 3D CFD simulation. As it is shown in Figure (a) which entails the experimental results, with increasing equivalence ratio LTRHR and HTRHR occur in advance. Section (b) is designed for the results of 3D CFD simulation.

With rising equivalence ratio HTRHR occurs earlier while LTRHR happens later. In the explanation of Figure 8, the maximum rate of n-heptane is introduced as the main factor of LTRHR. At this point, as it has shown with increasing equivalence ratio the maximum rate of n-heptane has happened later which has caused some issues in predicting the effect of equivalence ratio on LTRHR.

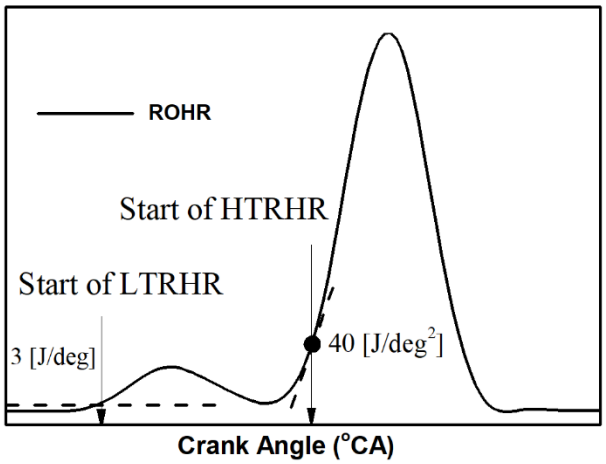

Figure 9: Definitions of the start of LTRHR and HTRHR

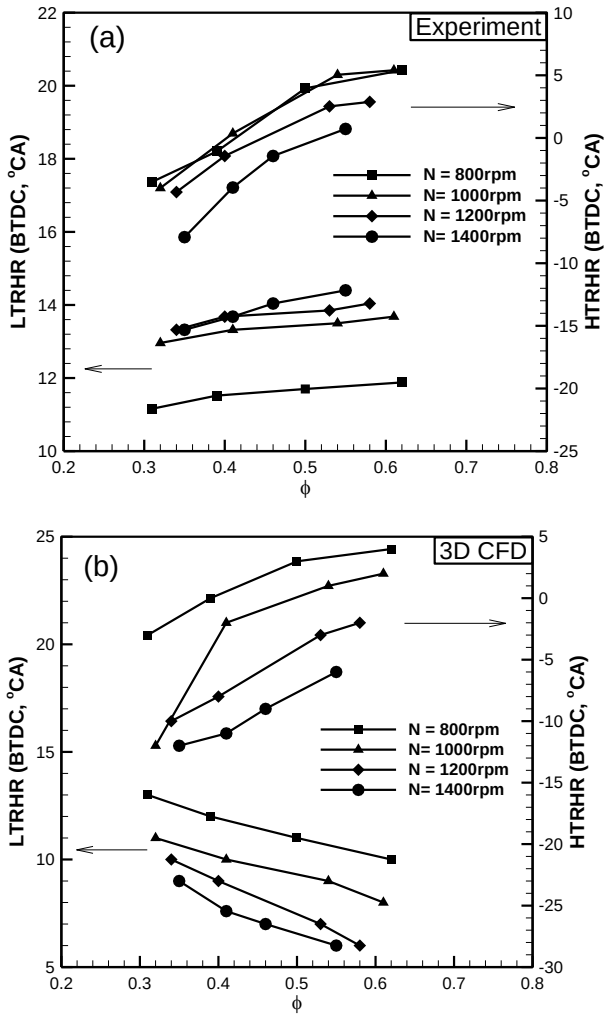

Figure 10: LTRHR and HTRHR for (a) experimental and (b) 3D CFD results

The impact of equivalence ratio on the values of P_{max} and crank angle related to P_{max} for all 16 operating conditions are inspected which is illustrated in Figure 11. For both simulating and experimental results, with increasing equivalence ratio the maximum value of P_{max} increases, and also the moment of occurrence of P_{max} happen in advance.

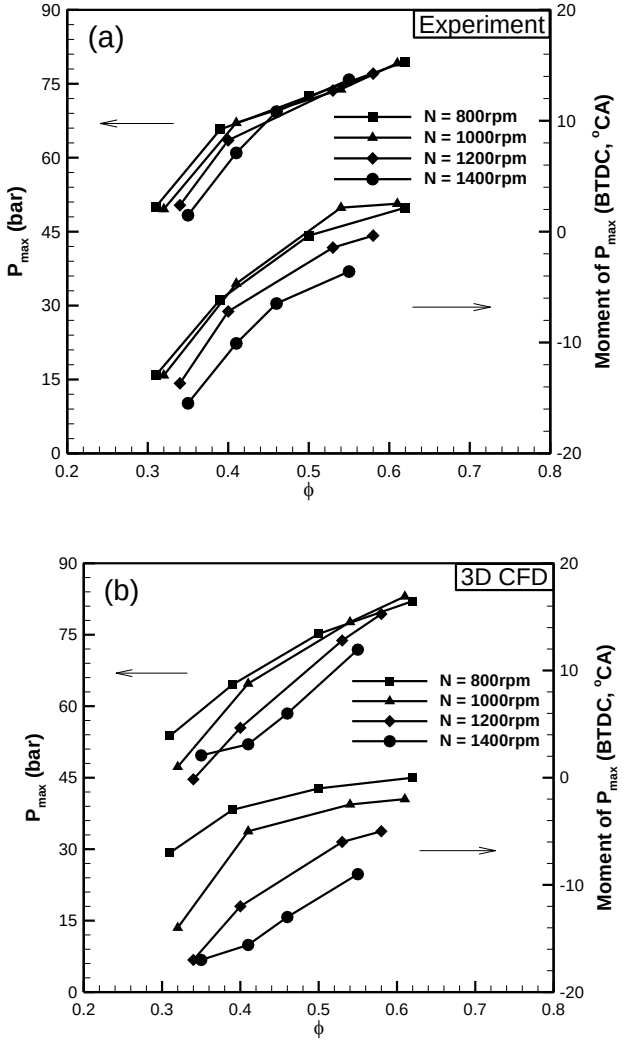

Figure 11: P_{max} and time of occurrence of P_{max} for (a) experimental and (b) 3D CFD results

In Figure 12., for the examined operating conditions, the impact of equivalence ratio on $ROHR_{max}$ and the moment of occurrence of $ROHR_{max}$ are provided. As it is obvious that with increasing equivalence ratio the maximum value of $ROHR_{max}$ increases and also the moment of occurrence of $ROHR_{max}$ happen in advance for both experimental and simulated results.

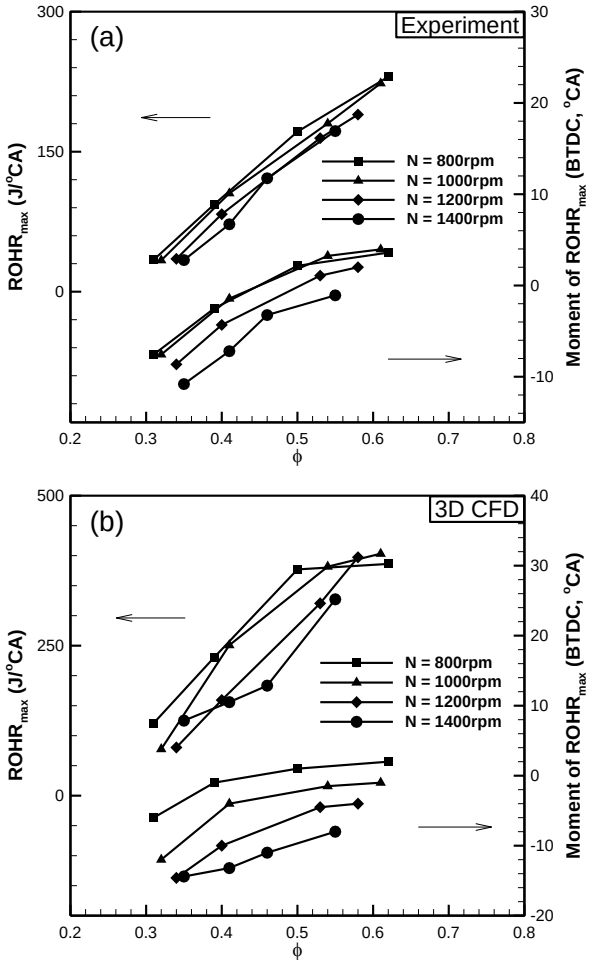

Figure 12: $ROHR_{max}$ and time of occurrence of $ROHR_{max}$ for (a) experimental and (b) 3D CFD results

5) Conclusions

In this research, the in-cylinder pressure and ROHR were studied in a broad range of HCCI engine operating states. To evaluate the changes of in-cylinder pressure and ROHR, 16 different operating conditions were specified.

The influence of the equivalence ratio was studied on the in-cylinder pressure and ROHR behaviors, LTRHR and HTRHR, rate of iso-octane and n-heptane, P_{max} and $ROHR_{max}$, and the crank angle related to P_{max} and $ROHR_{max}$, and the results were presented. The results of this study were obtained through experimental tests and 3D-CFD simulations coupled with chemical kinetics. The main findings of this research can be summarized as follows:

1. In the studied operating conditions, the experimental results indicated higher equivalence ratios, the maximum in-cylinder pressure, and the maximum ROHR increase.
2. The experimental results suggested that in the examined conditions, increasing the equivalence ratio advances both stages of

heat release (LTRHR and HTRHR) and also advances the time of occurrence of the maximum in-cylinder pressure and the maximum ROHR.

3. In the 3D-CFD simulations, the increase of the maximum pressure and ROHR with the rise of the equivalence ratio was properly observed.
4. The 3D-CFD simulations properly saw the combustion in all of the studied operating conditions.
5. By increasing the equivalence ratio, 3D-CFD simulations show advances in the time of occurrence of the maximum in-cylinder pressure and the maximum ROHR but mistakenly predicted the start of LTRHR more delayed, while the start of HTRHR was properly predicted.

List of Symbols

A	Arrhenius coefficient
C	mass concentration of species, kg
CA	Crank Angle, deg
E_a	activation energy, KJ/mole
H	specific enthalpy, J/kg
I	i^{th} species
K	reaction rate constant
k	turbulence kinetic energy, m/s^2
N	engine speed, rpm
N_R	number of reaction
N_s	number of species
P	In-cylinder pressure, Pa
$\dot{q}$	specific energy source production, W/kg
$\dot{r}$	species source production, kg/s
R_u	universal ideal gas constant, J/mole K
T	temperature, K
t	time, s
Y	species mass fraction, kg

Greek Symbols

β	Arrhenius coefficient
ε	weighted turbulence dissipation rate, kg/ms^3
θ	crank Angle, deg
λ	conduction coefficient, W/m K
μ	viscosity, kg/m s
μ_t	turbulence viscosity, kg/m s
ρ	density, kg/m^3
τ	shear stress tensor, Pa
$\dot{\omega}$	chemical species production rate, mol/cm^3s
$\nu'_{k,i}, \nu''_{k,i}$	stoichiometric coefficient of the k^{th} chemical species of i^{th} reaction in the forward and backward direction

Abbreviations

3D-CFD	Three-dimensional computational fluid dynamics
ABDC	After the bottom dead center
BBDC	Before the bottom dead center
COV	Coefficient of variations
DI	Direct injection
EGR	Exhaust gas recirculation
EVO	Exhaust valve opening
HCCI	Homogeneous charge compression ignition
HTR	High-temperature reaction
HTRHR	High-temperature reaction heat release
IVC	Intake valve closing
IMEP	Indicated mean effective pressure
ICE	Internal Combustion Engine
LTC	Low-temperature combustion
LTR	Low-temperature reaction
LTRHR	Low-temperature reaction heat release
NG	Natural gas
P_{max}	Maximum of pressure
$ROHR_{max}$	Maximum of the rate of heat release
RON	Research octane number
SOC	Start of combustion
TB	Third body

References

[1] M. Fathi and O. Jahanian, Fuel reactivity as a means to control DI-HCCI combustion engine, JER, Vol. 47, No. 47, pp. 39-46, 2017

[2] M. Fathi, D.D. Ganji and O. Jahanian, Intake charge temperature effect on performance characteristics of direct injection low-temperature combustion engines, Journal of Thermal Analysis and Calorimetry, Vol. 139, pp. 2447-2454, 2020

[3] H. Solmaz, A comparative study on the usage of fusel oil and reference fuels in an HCCI engine at different compression ratios, Fuel, Vol. 273, 117775, 2020
[4] M. Nazoktabar, S.A. Jazayeri, M. Parsa, D.D. Ganji and K. Arshtabar, Controlling the optimal combustion phasing in an HCCI engine based on load demand and minimum emissions, Energy, Vol. 182, pp. 82-92, 2019
[5] O. Jahanian, S. Jazayeri and A. Yousefzadeh, Developing a multi-zone thermo-kinetic model to investigate effects of using DME-methane blend in an HCCI engine, JER, Vol. 32, No. 32. pp. 37-47, 2013
[6] S.M. Ardebili, A. Taghipoor, H. Solmaz and M. Mostafaei, The effect of nano-biochar on the performance and emissions of a diesel engine fueled with fusel oil-diesel fuel, Fuel, Vol. 268, 117356, 2020
[7] A.H. Pour, S.M. Ardebili and M.J. Sheikhdavoodi, Multi-objective optimization of diesel engine performance and emissions fueled with diesel-biodiesel-fusel oil blends using response surface method, Environmental Science and Pollution Research, Vol. 25, pp. 35429-35439, 2018
[8] X. Lü, Y. Hou, L. Zu and Z. Huang, Experimental study on the auto-ignition and combustion characteristics in the homogeneous charge compression ignition (HCCI) combustion operation with ethanol/n-heptane blend fuels by port injection, Fuel, Vol. 85, pp. 2622-2631, 2006
[9] R.K. Maurya and A.K. Agarwal, Experimental investigation on the effect of intake air temperature and air–fuel ratio on cycle-to-cycle variations of HCCI combustion and performance parameters, Applied Energy, Vol. 88, pp. 1153-1163, 2011
[10] D. İpci, E. Yılmaz, F. Aksoy, A. Uyumaz, S. Polat and H. Solmaz, The Effects of iso-propanol and n-heptane Fuel Blends on HCCI Combustion Characteristics and Engine Performance, Makine Teknolojileri Elektronik Dergisi, Vol. 12, No. 1, pp. 49-56, 2015
[11] C. Cinar, A. Uyumaz, H. Solmaz, F. Sahin, S. Polat and E. Yilmaz, Effects of intake air temperature on combustion, performance and emission characteristics of a HCCI engine fueled with the blends of 20% n-heptane and 80% isooctane fuels, Fuel Processing Technology, Vol. 130, pp. 275-281, 2015
[12] S. Polat, An experimental study on combustion, engine performance and exhaust emissions in a HCCI engine fuelled with diethyl ether–ethanol fuel blends, Fuel Processing Technology, Vol. 143, pp. 140-150, 2016
[13] A. Calam, H. Solmaz, E. Yılmaz and Y. İçingür, Investigation of effect of compression ratio on combustion and exhaust emissions in A HCCI engine, Energy, Vol. 168, pp. 1208-1216, 2019
[14] H. Ezoji, R. Shafaghat and O. Jahanian, Numerical simulation of dimethyl ether/natural gas blend fuel HCCI combustion to investigate the effects of operational parameters on combustion and emissions, Journal of Thermal Analysis and Calorimetry, Vol. 135, pp. 1775-1785, 2019
[15] A. Dayal, M. Shrivastava, R. Upadhyaya and L.S. Brar, Numerical study using detailed chemistry combustion comparing effects of wall heat transfer models for compression ignition diesel engine, SN Applied Sciences, Vol. 1, 1005, 2019
[16] P.V. Shinde, R.G. Desavale, V.R. Patil, P.M. Gawali and S.M. Patil, Modeling, attenuation and flow field analysis of diesel engine muffler using fluid structure interaction approach and experimental analysis, SN Applied Sciences, Vol. 2, pp. 1-11, 2020
[17] R. Ogink and V. Golovitchev, Gasoline HCCI modeling: Computer program combining detailed chemistry and gas exchange processes, (No. 2001-01-3614), SAE Technical paper, 2001
[18] L. Noel, F. Maroteaux and A. Ahmed, Numerical study of HCCI combustion in diesel engines using reduced chemical kinetics of n-heptane with multidimensional CFD code, (No. 2004-01-1909), SAE Technical Paper, 2004
[19] Z. Wang, S.J. Shuai, J.X. Wang and F. Zhang, Numerical simulation of gasoline stratified charge compression ignition using 3D-CFD coupled with detailed chemistry, Combustion science and technology, Vol. 180, pp. 1295-1316, 2008
[20] K. Poorghasemi, R.K. Saray, K. Bahlouli and A. Zehni, 3D CFD simulation of a natural gas fueled HCCI engine with employing a reduced mechanism, Fuel, Vol. 182, pp. 816-830, 2016
[21] A. Yousefzadeh and O. Jahanian, Using detailed chemical kinetics 3D-CFD model to investigate combustion phase of a CNG-HCCI engine according to control strategy requirements, Energy Conversion and Management, Vol. 133, pp. 524-534, 2017
[22] J.B. Heywood, Internal Combustion Engine Fundamentals, McGraw-Hill Book Company, 1988
[23] AVL Fire user manual, CFD-Solver_v2008_05_CFD-Solver.
[24] H. Wang, M. Yao and R.D. Reitz, Development of a reduced primary reference fuel mechanism for internal combustion engine combustion simulations, Energy & Fuels, Vol. 27, pp. 7843-53, 2013
[25] K.K. Kuo, Principles of Combustion, John Wiley &Sons, New York, USA, 1986.

فصلنامهٔ علمی تحقیقات موتور

تارنمای فصلنامه: www.engineresearch.ir

ارزیابی اثرات نسبت هم‌ارزی بر احتراق موتور اشتعال تراکمی مخلوط همگن

مسعود رابطی[۱]، امید جهانیان[۲*]، علی اکبر رنجبر[۳]، سید محمد صفی الدین اردبیلی[۴]، حمیت سولماز[۵]

[۱] دانشجوی دکتری، دانشگاه صنعتی نوشیروانی بابل، بابل، ایران، masoud.rabeti@gmail.com
[۲] دانشیار، دانشگاه صنعتی نوشیروانی بابل، بابل، ایران، jahanian@nit.ac.ir
[۳] استاد، دانشگاه صنعتی نوشیروانی بابل، بابل، ایران، ranjbar@nit.ac.ir
[۴] استادیار، دانشگاه شهید چمران اهواز، اهواز، ایران، m.safieddin@scu.ac.ir
[۵] دانشیار، دانشگاه غازی، آنکارا، ترکیه، hsolmaz@gazi.edu.tr
[*] نویسندهٔ مسئول

چکیده

در این مقاله در ۱۶ حالت عملکردی اثر نسبت هم‌ارزی بر ویژگی‌های احتراقی بررسی شده است. سوخت استفاده شده در این تحقیق بنزین بود و اشتعال در دو مرحله صورت گرفت. مرحلهٔ اول اشتعال وابسته به آزادسازی انرژی واکنش‌های دما سرد و مرحلهٔ دوم وابسته به آزادسازی انرژی واکنش‌های دما داغ بوده است. شبیه‌سازی سه‌بعدی دینامیک سیالات محاسباتی با در نظرگرفتن جزئیات شیمیایی به عنوان روش عددی انتخاب شده است. در تمام آزمایش‌های انجام شده، شبیه‌سازی سه‌بعدی دینامیک سیالات محاسباتی احتراق را به خوبی و به طور کامل نشان داده است. همچنین با افزایش نسبت هم‌ارزی، الگوی سه‌بعدی جلو افتادن زمان وقوع بیشینه فشار و بیشینه آزادسازی انرژی را نشان داده است اما به اشتباه شروع آزادسازی انرژی واکنش دما سرد را با تأخیر تخمین زده در حالی‌که شروع آزادسازی انرژی واکنش دما داغ را به درستی پیش‌بینی کرده است.

اطلاعات مقاله

تاریخچهٔ مقاله:
دریافت: ۱۵ آذر ۱۳۹۹
پذیرش: ۲۷ دی ۱۳۹۹

کلیدواژه‌ها:
احتراق اشتعال تراکمی مخلوط همگن
شبیه‌سازی دینامیک سیالات محاسباتی
نسبت هم‌ارزی
آزادسازی انرژی واکنش دما سرد
آزادسازی انرژی واکنش دما داغ